Aqueous solution-processed AlO_x dielectrics and their biased radiation response investigated by an on-site technique

Yuxiao Fang [1], Chun Zhao [1,2,*], Stephen Hall [1], Ivona Z. Mitrovic [1], Wangying Xu [3], Li Yang [4,5], Tianshi Zhao [1], Qihan Liu [1] and Cezhou Zhao [1,2,*]

[1] Department of Electrical Engineering and Electronics, University of Liverpool, Liverpool L69 3GJ, UK;
[2] Department of Electrical and Electronic Engineering, Xi'an Jiaotong-Liverpool University, Suzhou 215123, China;
[3] College of Materials Science and Engineering, Guangdong Research Center for Interfacial Engineering of Functional Materials, Shenzhen Key Laboratory of Special Functional Materials, Shenzhen University, Shenzhen 518060, China;
[4] Department of Chemistry, Xi'an Jiaotong-Liverpool University, Suzhou 215123, China;
[5] Department of Chemistry, University of Liverpool, Liverpool L69 7ZD, UK;
[*] Correspondence: E-mail: Chun.Zhao@xjtlu.edu.cn, Cezhou.Zhao@xjtlu.edu.cn

Abstract: The effect of annealing temperature on the properties of aqueous solution-processed AlO_x thin films is reported in this paper. Specifically, the stability of AlO_x based Metal Oxide Semiconductor (MOS) capacitor devices under bias-stress (BS) and biased radiation stress (BRS) were assessed by an on-site technique with bias stress time up to 10^5 s. A 662-keV Cs^{137} γ-ray radiation source was used, with circa 92 Gy, for biased radiation stress experiments. In order to better understand the origin of degradation mechanisms, the build-up of charge and generation of defects during the BS and BRS were analyzed by calculation of the variation of oxide trap density (ΔN_{ot}) in AlO_x bulk and interface trap density (ΔN_{it}) at the oxide/semiconductor interface. It is been found that high annealing temperature (>250 °C) can result in the formation of AlO_x thin films with reduced impurities, low leakage current, and satisfactory BS as well as BRS stability. The results of ΔN_{ot} and ΔN_{it} vs stress time indicate that AlO_x bulk oxide traps dominate the shift of flat-band voltage (V_{FB}) under BRS. Furthermore, ΔN_{ot} and ΔN_{it} decrease slightly under positive biased radiation stress (PBRS), while the increase in ΔN_{ot} and ΔN_{it} concentrations observed under negative biased radiation stress (NBRS), exhibits a mechanism which differs from the traditional two-stage process theory.

Keywords: Solution-processed; High-k gate dielectric; AlO_x capacitor; Biased γ-ray radiation stress stability; On-site radiation measurements

1. Introduction

To date, metal-oxide thin-film transistors (TFTs) have attracted considerable attention for next generation display technology due to their high optical transparency, excellent charge transport characteristics, good chemical stability, and high mechanical tolerance [1-7]. Compared to traditional vacuum thin film deposition methods, solution processes enable the fabrication of larger area flexible low-cost metal-oxide TFTs due to advantages of simplicity, low-cost and high throughput. Over the past decade, solution-processed thin film deposition techniques for oxide materials have been well developed, including dip-coating, spin-coating and inkjet-printing [8-15]. In addition, solution-processed high-*k* dielectrics such as Al_2O_3, ZrO_2, La_2O_3 and HfO_2 in TFTs have been utilized to achieve low operation voltage and gate leakage current [2,9-11,15-24]. Among the various high-*k* dielectrics, Al_2O_3 is considered to be an excellent candidate due to its high breakdown field, good thermal and chemical stability, relatively high dielectric constant, smooth surface and amorphous structure under typical processing conditions [1,11,20,22,25,26]. Most of the solution-processed AlO_x thin films are currently fabricated by toxic organic precursor solvents such as 2-methoxyethanol and acetonitrile. These precursor solvents could induce the potential environmental damage within the processing procedures. Since water can be implemented as a suitable precursor solution, aqueous solution-processed AlO_x dielectric could be a promising alternative candidate for the application in eco-friendly, low-cost and low power consumption TFT devices [1,11,18,25].

Furthermore, solution-processed oxide TFTs are crucial to enable large-area electronics in harsh radiation environments, such as whole-body-scanning X-ray detectors and large-area antenna arrays [27]. Only a few studies have addressed radiation damage in solution-processed high-*k* dielectrics for TFT applications [27]. Typically, ionizing radiation can generate bulk oxide and interface traps near the oxide/semiconductor interface, which cause device degradation [28]. In addition, the applied voltage bias stress (BS) on TFT devices will enhance the motion, reactions, and trapping of charge at or near the oxide/semiconductor interface [29]. Therefore, the long-term reliability of solution-processed devices under biased radiation stress (BRS) needs to be investigated. The electrical characteristics of devices have been evaluated before and after irradiation via conventional off-site radiation response method. The ineluctable interruption of irradiation can cause a rapid recovery of flat band voltage (V_{FB}) shift, which leads to underestimation of the degradation caused by charge trapping/de-trapping. Consequently, on-site measurements have been introduced to fully characterize radiation induced degradation. There has been limited research reported on the γ-ray radiation response of solution-processed high-*k* dielectrics by on-site techniques.

In this work, the effect of annealing temperature in the range 150-300 ^{o}C on physical and chemical properties of solution processed AlO_x thin films were investigated by spectroscopic ellipsometry, thermogravimetric analysis-differential scanning calorimetry (TGA-DSC), atomic force microscopy (AFM), X-ray diffraction (XRD) and Fourier transform infrared spectroscopy (FT-IR). In order to investigate the electrical properties comprehensively, AlO_x thin films were integrated into Metal Oxide Semiconductor (MOS) capacitors. Capacitance-frequency (C-*f*), capacitance-voltage (C-V), leakage current-voltage (J_{leak}-V) and flat-band voltage shift (ΔV_{FB}) measurements were carried out. Furthermore, BS and BRS stability were systemically investigated by an on-site technique. The measurements were carried out under continuous γ-ray exposure with various gate bias stresses. In order to investigate the origin of degradation mechanisms, the build-up of charge and the generation of defects during the BS and BRS were analyzed by calculating the variation of oxide trap (ΔN_{ot}) and interface trap density (ΔN_{it}). The results of ΔN_{ot} and ΔN_{it} suggest that oxide AlO_x bulk traps dominated the shift of the V_{FB}. Furthermore, ΔN_{ot} and ΔN_{it} increase in magnitude under negative biased radiation stress (NBRS) and decrease under positive biased radiation stress (PBRS).

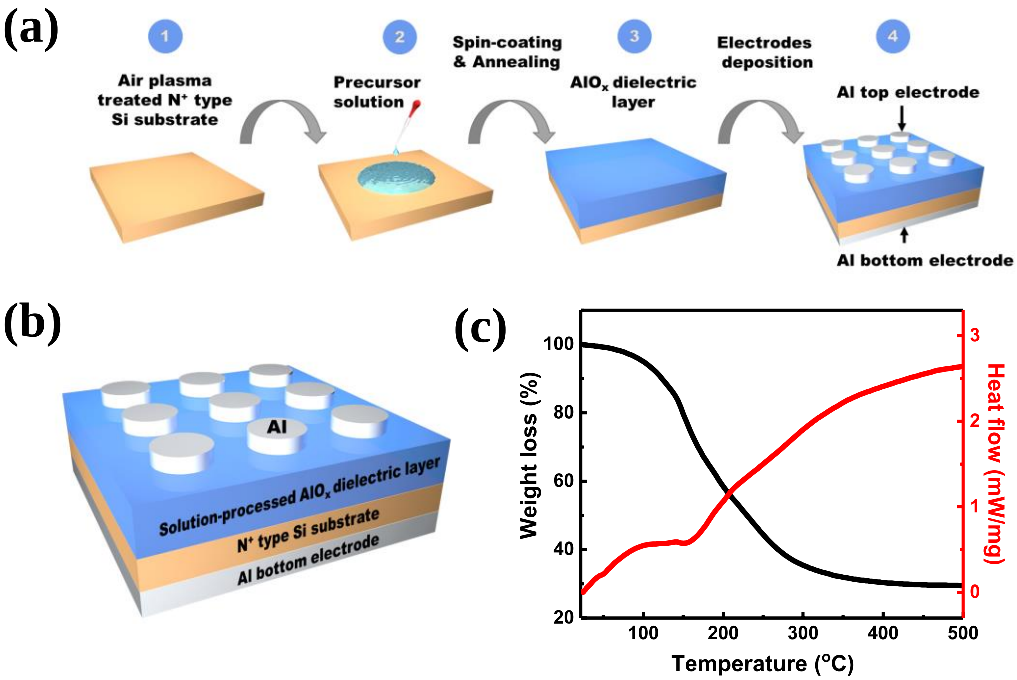

Figure. 1 **(a)** Fabrication process of solution-processed AlO_x Metal Oxide Semiconductor (MOS) capacitor. **(b)** A cross-section of solution-processed AlO_x MOS capacitor with a structure of Al/N^+-Si/AlO_x/Al from bottom to top. **(c)** Thermogravimetric analysis-differential scanning calorimetry (TGA-DSC) curves of $Al(NO_3)_3$ precursor powder heated from 20 °C to 500 °C with a heating rate of 10 °C/min.

2. Experimental

2.1 Precursor Preparation

The fabrication process and a cross-section of the AlO_x MOS capacitor are shown in Figs. 1(a) and (b), respectively. To prepare the precursor solution, aluminum nitrate hydrate ($Al(NO_3)_3{\cdot}xH_2O$) was dissolved in water to produce a colorless and clear solution with 2.5 M molar concentration. The solution was stirred in ultrasonic bath for 2 h to ensure the precursor was fully dissolved since the nitrate salts show excellent water solubility. Then the solution was filtered by a 0.45 µm polyether sulfone (PES) syringe filter before spin coating.

2.2 Device fabrication

To prepare the substrates, lightly-doped N type Si substrates (resistivity: 2-4 Ω·cm) were dipped in 2% HF aqueous solution for 60 s to remove the native oxide and then dried by N_2. Subsequently, the substrates were exposed under air plasma for 15 mins. After preparation of Si substrates, the precursor solution was spin-coated on the processed substrate at 4500 rpm for 40 s and then annealed on the hot plate at temperatures of 150 °C, 200 °C, 250 °C and 300 °C for 1 h. Finally, 300 nm thick Al top and bottom electrodes were deposited through shadow masks by e-beam evaporation. The circular top electrode had a diameter of 0.3 mm.

2.3 Characterization

The thickness of the solution-processed AlO_x thin films was measured by spectroscopic ellipsometry. To investigate the thermal behavior of the precursor powder, the precursor solution was dried at 100 °C for 1 h and then monitored by TGA-DSC. The thin film morphologies were characterized by atomic force microscopy in tapping mode. The structural and crystal properties were characterized by X-ray diffraction. The chemical characteristics of AlO_x thin films were investigated by FT-IR. The C-V characteristics were measured using a HP 4284 precision LCR meter at a frequency of 1 MHz. To investigate the BS and BRS stability of AlO_x MOS capacitor, constant voltage bias stress was applied on the gate with and without radiation exposure. During the bias-stress, C-V curves were measured at regular points in time of $10^{1/3}$ s, $10^{2/3}$ s, $10^{3/3}$ s, $10^{4/3}$ s, $10^{5/3}$ s etc. to allow extraction of the V_{FB}. For BRS, a 662-keV Cs^{137} γ-ray radiation source was used, the stress time was up to 10^5 s and the total dose was around 92 Gy. All electrical measurements were carried out in the dark at room temperature.

3. Results and Discussion

3.1 Annealing Temperature Effect

Fig. 1(c) displays the thermal behavior of AlO_x precursor powder. The measurement temperature increased from 20 °C to 500 °C with a heating rate of 10 °C/min. It can be seen that the weight of precursor powder decreases abruptly from 100 °C to 280 °C, which is likely to be due to the evaporation of the solvent, decomposition of the impurities and hydrolysis of the metal precursors of AlO_x precursor powder. After 280 °C, the gradual weight loss of precursor powder indicates that the residual of the solvent and impurities of the precursor powder (such as nitrate) have been almost eliminated. The TGA-DSC results prove that the 300 °C annealing temperature is high enough to form the metal oxygen metal frame, densify the films, and eliminate precursor impurities in the AlO_x layer. Table 1 summarizes the microstructural and dielectric properties of solution-processed AlO_x dielectrics under various annealing temperatures, including thickness, roughness, leakage current at 6 V, areal capacitance at 1 kHz and dielectric constant at 1 kHz.

3D AFM images of solution-processed AlO_x thin films annealed at different temperatures are shown in Fig. 2. The root-mean-square (rms) roughness values of all AlO_x thin films are found to be in the range of 0.1~0.2 nm, indicating that AlO_x thin films have an ultra-smooth surface when annealed up to 300 °C. Low surface roughness is a critical feature of the gate dielectric in high performance TFTs, since it allows low leakage current and facilitates high carrier mobility in the transistor channel [11,20].

Table 1. Microstructural and dielectric properties of solution-processed AlO_x thin films.

Annealing Temperature (°C)	**Thickness (nm)**	**Roughness (nm)**	**Leakage Current at 6 V (A/cm²)**	**Areal Capacitance (nF/cm²) at 1 kHz**	**Dielectric Constant at 1 kHz**
150	60	0.14	2.6×10^{-5}	102	7.0
200	54	0.11	5.0×10^{-6}	132	8.1
250	52	0.19	3.5×10^{-6}	139	8.2
300	45	0.2	2.6×10^{-6}	171	8.7

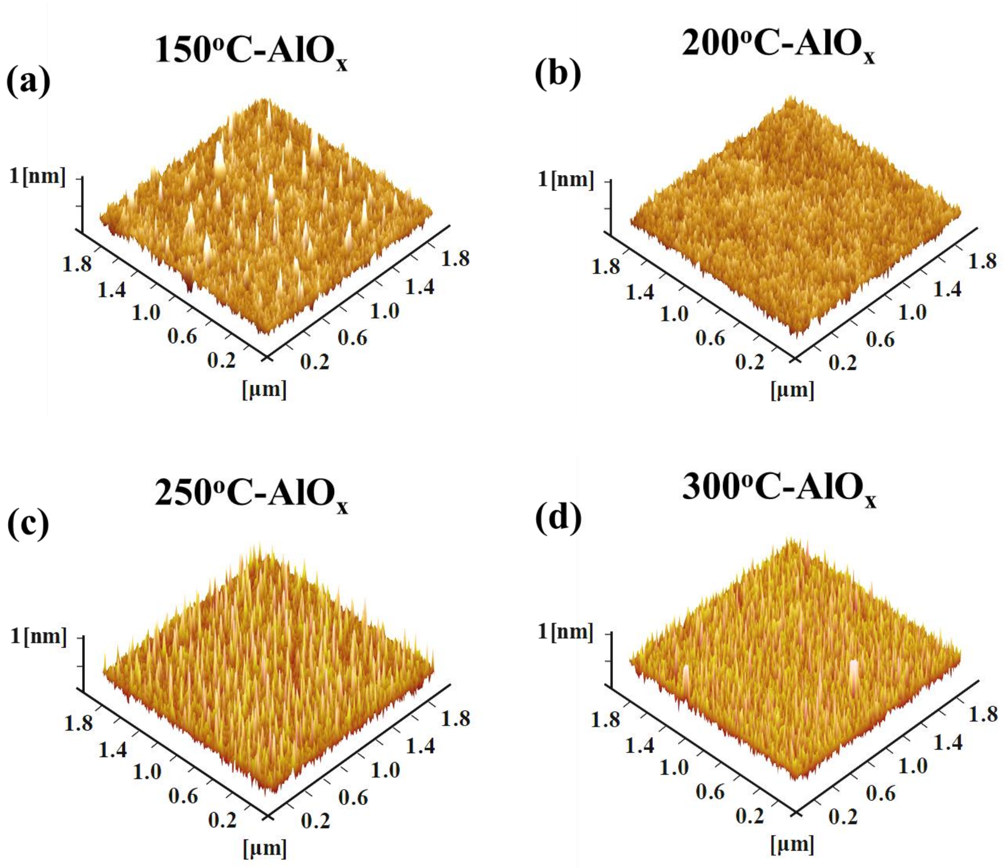

Figure 2. 3D AFM images of solution-processed AlO_x thin films annealed at **(a)** 150 ^{o}C, **(b)** 200 ^{o}C, **(c)** 250 ^{o}C and **(d)** 300 ^{o}C. The image dimensions are 1.8 μm × 1.8 μm.

Fig. 3(a) shows the XRD spectra of AlO_x thin films annealed at different temperatures. No peaks corresponding to the crystalline AlO_x are observed in Fig. 3(a), which confirms that AlO_x films remain amorphous up to 300 ^{o}C. The amorphous structure allows for low leakage current and higher breakdown voltage. Conversely, poly-crystalline films allow enhanced leakage current and impurity diffusion via grain boundaries [14,30,31]. The FT-IR spectra for the solution-processed AlO_x thin films are shown in Fig. 3(b). The broad peaks in the range of 3000-3600 cm^{-1} are likely to be related to hydroxyl (O-H) group stretching vibrations [32]. The peaks in the 1300–1500 cm^{-1} range represent nitrate (NO^{3-}) group deformation vibrations [22,32,33]. As the annealing temperature increases, these two peaks diminish, which is ascribed to the evaporation of the solvent and the gradually decomposition of O-H and NO^{3-} groups in thin films. The bands in the range of 750–900 cm^{-1} are due to vibrations of Al-O bond. It low temperature (<200 ^{o}C) annealed conditions, the Al-O bond is not formed and only weak absorptions of hydrated metal nitrate species are observed [34]. At annealing temperature >250 °C, Al-O bond is configured. Consequently, 300 ^{o}C is high enough to remove the solvent residue and impurities, as well as the formation of the metal-oxide framework, in agreement with the TGA-DSC results shown in Fig. 1(c).

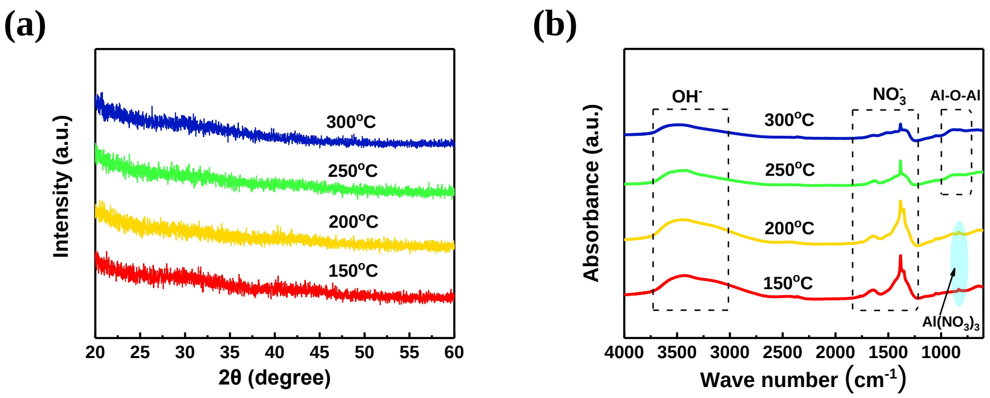

Figure 3. **(a)** XRD patterns and **(b)** FT-IR spectra of solution-processed AlO_x thin films annealed at different temperatures.

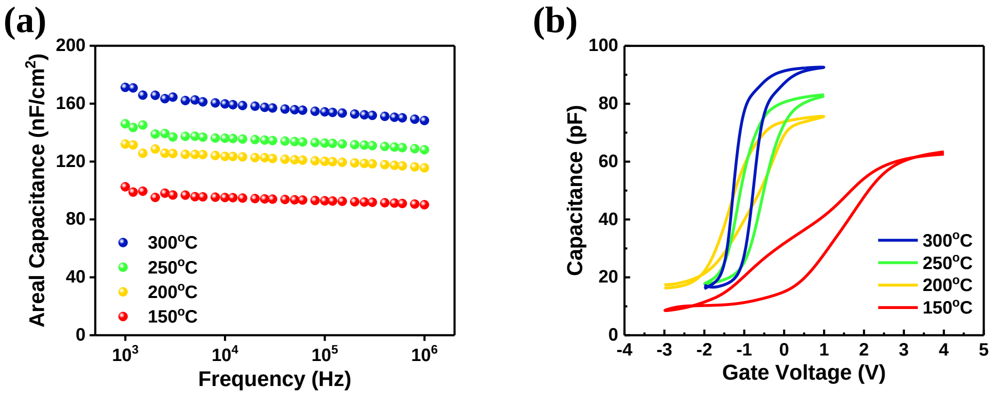

Figure 4. **(a)** Capacitance-frequency (C-*f*) and **(b)** capacitance-voltage (C-V) characteristics of solution-processed AlO_x MOS capacitors annealed at 300, 250, 200 and 150 °C.

Fig. 4(a) shows the areal C-*f* plots for AlO_x MOS capacitors. It can be seen that the areal capacitance increases with the rise in annealing temperature. This can be attributed to the formation of the metal-oxide framework and its densification at high annealing temperatures [11,14]. The dielectric constants of AlO_x thin films were calculated using the capacitance values measured at 1 kHz (see Table 1) and are consistent with values reported for solution-processed AlO_x [19,25]. Furthermore, the capacitance decreases as the frequency increases from 1 kHz to 1 MHz. In general, the capacitances fabricated in a vacuum environment show quite small frequency dispersion compared to those fabricated in ambient environment [33]. It has been shown that the electrical double layer (EDL) formed by mobile H^+ in AlO_x film has a strong effect on the measured capacitance at low frequencies. This is due to the slow migration rate of protons in response to low measurement frequency [14] [35]. The 300 °C annealed AlO_x thin film is found to have the weakest frequency dispersion, indicating a low density of impurity H^+. The C-V characteristics of AlO_x MOS capacitors measured at 1 MHz are shown in Fig. 4(b). Since the slope of the CV curves in the depletion region reflects the interface trap density, it can be seen that the slope increases with increasing annealing temperature, indicating a decrease in interface trap density. This could be due to the evaporation of hydroxyl groups and residual nitrate, the decomposition of metal

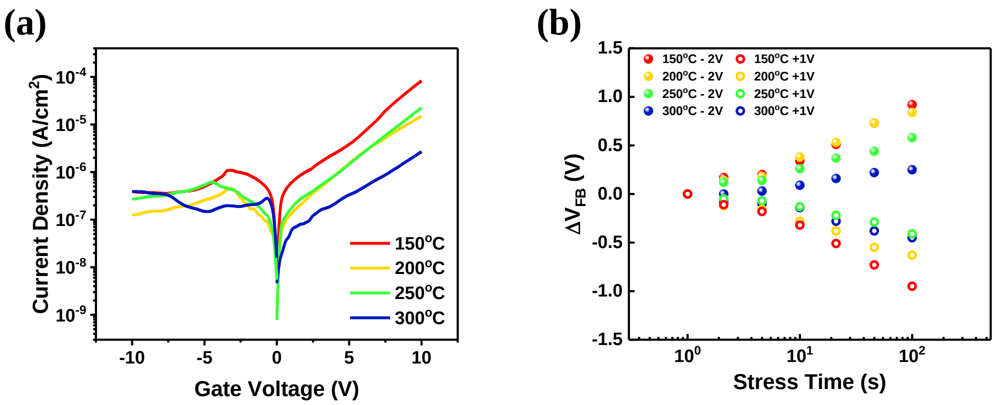

Figure 5. **(a)** Leakage current density-gate voltage (J_{leak}-V) and **(b)** flat-band voltage shift (ΔV_{FB}) vs stress time of solution-processed AlO_x MOS capacitors annealed at different temperatures. ΔV_{FB} are extracted from C-V curves measured from MOS capacitors at 1 MHz under different gate bias-stresses. The area of the capacitors is 7.1×10^{-4} cm^2

precursor and the formation of the metal-oxide framework under high annealing temperature [2,10,20,33].

The leakage current density–gate voltage (J_{leak}-V) measurements were performed to evaluate the leakage behavior of AlO_x thin films, as shown in Fig. 5(a). It can be seen that J_{leak} decreases with increasing anneal temperature. The 150 °C-AlO_x thin film has a J_{leak} of 2.6 $\times10^{-5}$ A/cm^2 at 6 V, which is relatively high compared to the thin films annealed at 200, 250 and 300 °C. This indicates that the AlO_x annealed at 150 °C suffers from an incomplete decomposition of precursor solution and therefore contains hydroxyl (O-H) and nitrate (NO^{3-}) groups, as shown in Fig. 3(b). The latter provide leakage current paths and result in a high J_{leak} [11] [36]. The 200 °C-AlO_x, 250 °C-AlO_x and 300 °C-AlO_x thin films all show quite low J_{leak} at 6 V; namely 5.0 × 10^{-6} A/cm^2, 3.5 $\times10^{-6}$ A/cm^2 and 2.6 × 10^{-6} A/cm^2, as shown in Table 1) [19]. This low leakage could be attributed to the decomposition of metal precursor as well as the formation of the metal-oxide framework [2,10,20].

The BS stability of AlO_x MOS capacitors annealed at different temperatures is assessed from flat-band voltage shifts under 100s BS, as shown in Fig. 5(b). To calculate ΔV_{FB}, V_{FB} are extracted from C-V curves measured at regular intervals (typically $10^{1/3}$ s, $10^{2/3}$ s, $10^{3/3}$ s, $10^{4/3}$ s, $10^{5/3}$ s…) during the BS. It can be seen that the 300 °C-AlO_x MOS capacitor has the minimum ΔV_{FB} under positive bias-stress (PBS) and negative bias-stress (NBS), and hence shows the best BS stability. This is likely to be due to its low defect density and high metallic oxide concentration, in agreement with the results of TGA-DSC (Fig. 1(c)), AFM (Fig. 2), FT-IR (Fig. 3(b)) and J_{leak}-V_g (Fig. 5(a)) shown earlier.

3.2 Biased Radiation Response

It can be concluded from the results above, that the 300 °C-AlO_x thin films have the best film quality, as indicated by their low defect density, high metallic oxide concentration, low leakage current and BS stability. Further radiation investigation of the BS and BRS stability of 300 °C-AlO_x MOS capacitors are now investigated in detail. Figs. 6(a) and (b) show the C-V curves of 300 °C-AlO_x MOS capacitors under PBS and NBS with stress time up to 10^5 s, respectively. For comparison, the C-V curves under PBRS and NBRS with total dose of around 92 Gy are shown in Figs. 6(c) and (d). It can be seen that the shift

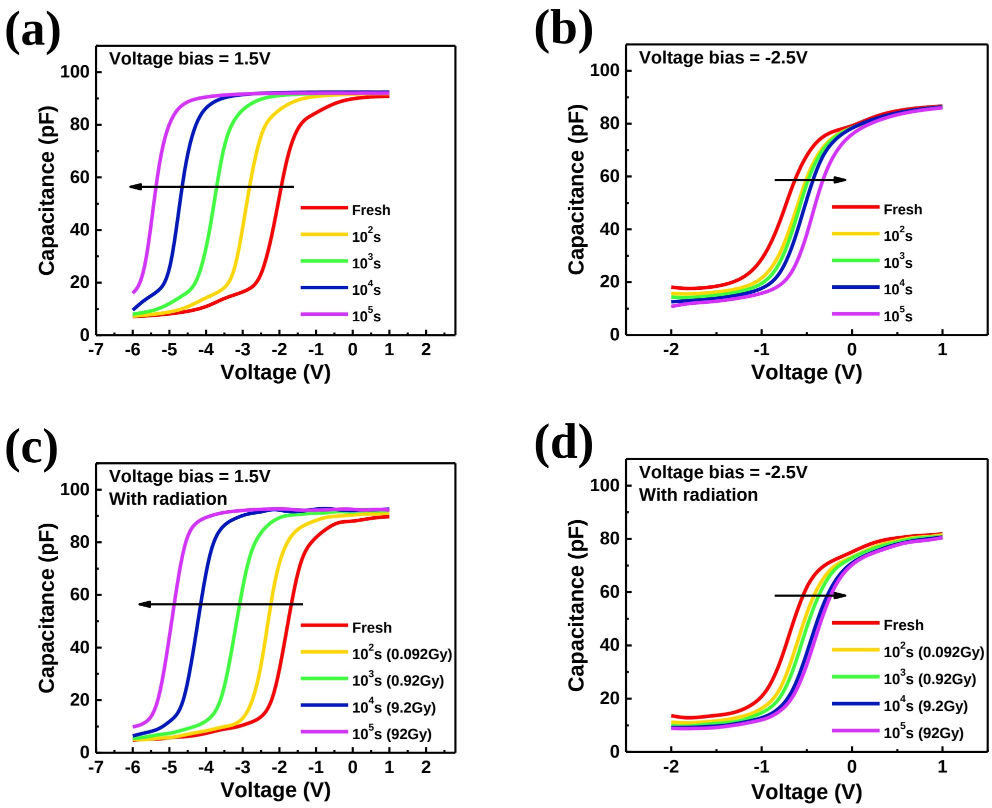

Figure 6. C-V curves of solution-processed 300 °C-AlO_x MOS capacitors under gate voltage of **(a)** +1.5 V, **(b)** -2.5 V, **(c)** irradiated +1.5 V and **(d)** irradiated -2.5 V with 10^5 s bias-stress time. The total dose is around 92 Gy.

of the C-V curves, positive or negative, is determined by the gate bias stress polarity. PB and NB produce negative and positive ΔV_{FB}, respectively. Positive ΔV_{FB} can be ascribed to the electron trapping in the AlO_x bulk and the passivation of the AlO_x/Si interface, while negative ΔV_{FB} is believed to be caused by proton trapping in the AlO_x bulk as well as the generation of Si dangling bonds at the AlO_x/Si interface. It is also observed that radiation exposure have effects on the shifts of the C-V curves under BRS, which is likely to be due to radiation induced electron-hole pair generation facilitating the charge trapping/de-trapping behavior in the AlO_x bulk, as well as the passivation/de-passivation of the AlO_x/Si interface.

Figs. 7(a) and (b) summarize the ΔV_{FB} of 300 °C-AlO_x MOS capacitor under 10^5 s BS and BRS, respectively. The device shows less ΔV_{FB} under NBS than under PBS with/without radiation, indicating better NBS stability than PBS stability. As shown in Fig. 7(b), the radiation is observed to cause a positive ΔV_{FB} under both PBRS and NBRS, which is likely to be induced by the formation of negatively charged states and/or the build-up of interface traps with the assistance of radiation. The comprehensive mechanism is discussed below. Furthermore, radiation barely affects ΔV_{FB} without bias-stress due to the radiation induced electron-hole pairs having no significant effect on device properties without an applied electric field [37]. ΔN_{ot} causes a parallel shift of both mid-gap and flat band voltages, while ΔN_{it} only causes ΔV_{FB} due to the stretch-out of the C-V curve. Consequently, ΔV_{FB} is attributed to the combined effect of generation of oxide traps in AlO_x and interface traps near the AlO_x/Si interface. As shown in

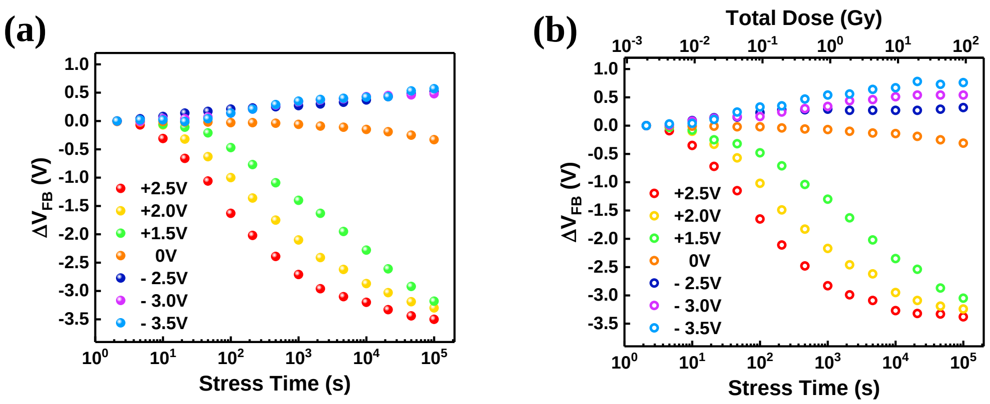

Figure 7. Flat band voltage shift (ΔV_{FB}) of solution-processed 300 °C-AlO_x MOS capacitors induced by different bias-stresses as a function of **(a)** stress time, **(b)** stress time & total dose.

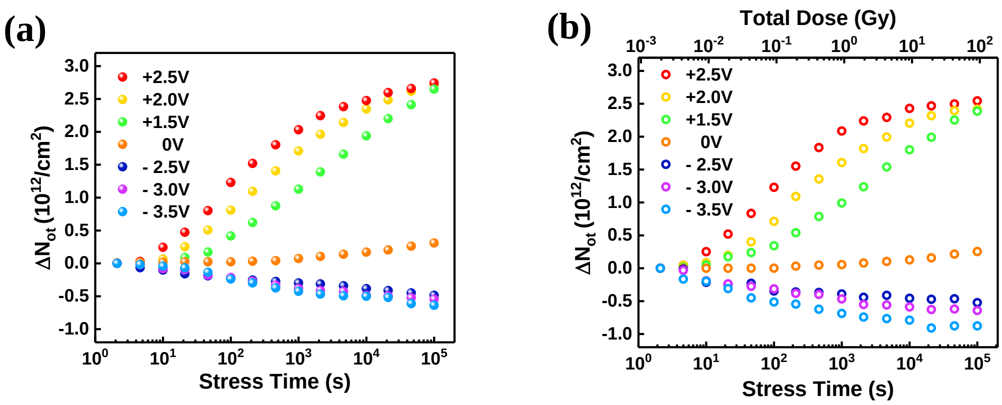

Figure 8. Variation of oxide traps density (ΔN_{ot}) of solution-processed 300 °C-AlO_x MOS capacitors induced by different bias-stresses as a function of **(a)** stress time, **(b)** stress time & total dose. ΔN_{ot} are extracted from mid-gap voltage shift (ΔV_{mg}) of C-V curves measured from 300 °C-AlO_x MOS capacitors at 1 MHz.

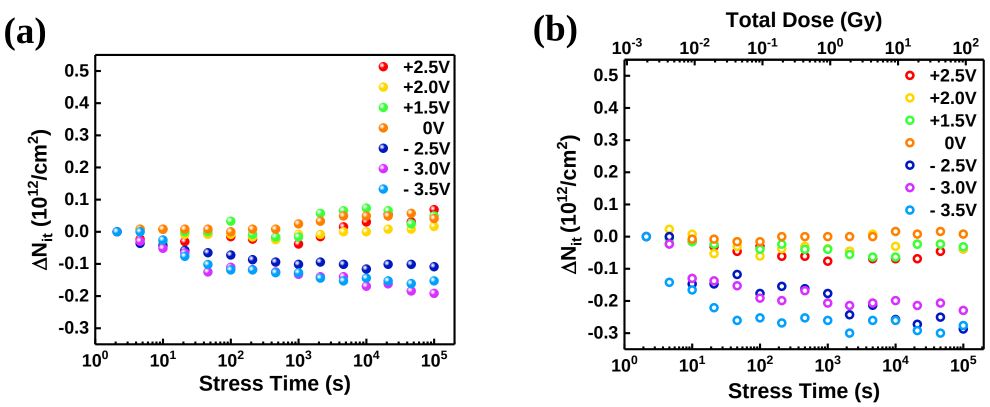

Figure 9. Variation of interface traps density (ΔN_{it}) of solution-processed 300 °C-AlO_x MOS capacitors induced by different bias-stresses as a function of **(a)** stress time, **(b)** stress time & total dose. ΔN_{it} are extracted from the difference between ΔV_{FB} and ΔV_{mg} of C-V curves measured from 300 °C-AlO_x MOS capacitors at 1 MHz.

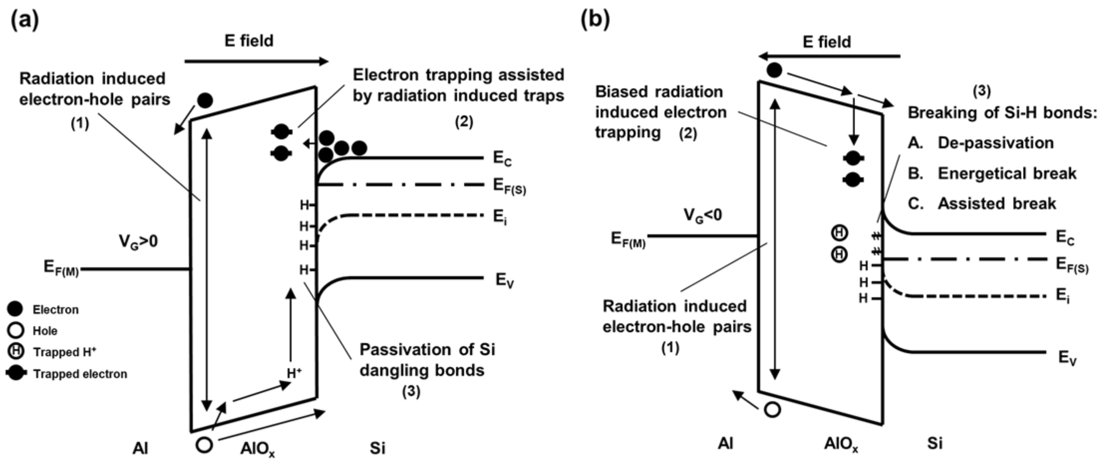

Figure 10. Energy band diagrams of solution-processed 300 ºC-AlO_x MOS capacitors under **(a)** positive biased radiation stress (PBRS) and **(b)** negative biased radiation stress (NBRS).

Fig. 8, ΔN_{ot} can be estimated by equation (1) [38]:

$$\Delta N_{ot} = -\frac{C_{ox}\Delta V_{mg}}{qA} \tag{1}$$

where ΔV_{mg} is the mid-gap voltage shift obtained from C-V curves, C_{ox} is the gate capacitance, q is the electronic charge, and A is the electrode area. It is notable that, under NBRS, ΔN_{ot} increases with increasing radiation dose and there is a net negative oxide trapped charges induced by BRS.

As shown in Fig. 9, ΔN_{it} can be estimated by equation (2) [38]:

$$\Delta N_{it} = \frac{C_{ox}(\Delta V_{FB} - \Delta V_{mg})}{qA}. \tag{2}$$

It can be seen that radiation can generate negative interface traps under all measurement conditions. Furthermore, for all total doses, ΔN_{ot} and ΔN_{it} are in the order of 10^{-12} and 10^{-11} cm^{-2} and no significant variation of N_{it} was observed compared to N_{ot}, indicating that oxide traps dominate the shift of V_{FB}. Such a high level of N_{ot} is likely to be due to hydrogen reactions. Similar results have been reported on high-*k* dielectric based MOS capacitors. Kahraman et al. have reported Gd_2O_3 MOS capacitors with ΔN_{ot} = 2.3×10^{-12} and ΔN_{it} =2.5×10^{11} after circa 50 Gy γ-ray exposure in [39] and Er_2O_3 MOS capacitors with ΔN_{ot} (1.3×10^{12}) and ΔN_{it} (9.4×10^{10}) after circa 78 Gy γ-ray exposure in [40].

As shown in Figs. 8 and 9, compared to BS, ΔN_{ot} and ΔN_{it} are found to decrease slightly under PBRS, while they increase in magnitude under NBRS. Under PBRS, the reduced ΔN_{ot} is ascribed to the combined effect of bias-stress and radiation exposure with increasing stress time. As shown in Fig. 10(a), neutral oxide traps are created in the bulk of the AlO_x during exposure to ionizing irradiation [41]. With a positively applied gate voltage, electrons in the accumulation region at the AlO_x/Si interface can tunnel from Si substrate into those radiation induced neutral oxide traps (process (2) in Fig. 10(a)). The effects of radiation exposure and gate voltage add up and negatively charged traps are formed accordingly as the BRS time increased, which can thus partially compensate the positive oxide trapped charges near the AlO_x/Si interface, thus reduce positive ΔN_{ot} [42,43].

The decrease ΔN_{it} under PBRS could be explained by the conventional two-stage process theory originally described by McLean [44]. As depicted in Fig. 10(a), in the first stage, as radiation passes through a gate oxide, electron-hole pairs are created within the gate dielectric (process (1) in Fig. 10 (a)) [45]. The radiation induced electrons escape from the oxide within several picoseconds due to their higher mobility compared to the holes. Meanwhile, the radiation induced holes move towards the AlO_x/Si interface under PBRS. Thereafter, in the second stage, hydrogen will be liberated during the transport of holes, in the form of protons (H^+) [29], and reach the interface via a hopping transport. The H^+ can then passivate the existing Si dangling bonds (Si^-) via reaction (3) listed below (process (3) in Fig. 10(a)). Once a defect is passivated by hydrogen, it no longer functions as an interface trap, therefore ΔN_{it} is reduced accordingly. Meanwhile, the Si-H bonds at the AlO_x/Si are also de-passivated by protons through reaction (4):

$$Si^- + H^+ \rightarrow Si - H \quad (3)$$

$$Si - H + H^+ \rightarrow Si^+ + H_2 \quad (4)$$

$$Si - H \rightarrow Si^- + H^+ \quad (5)$$

Nevertheless, the high concentration of protons and Si dangling bonds near the AlO_x/Si interface could cause a higher probability for protons to passivate Si dangling bonds via reaction (3), rather than to de-passivate a Si-H bond and form an interface trap via reaction (4) [46-48].

The mechanism for the increase of ΔN_{ot} and ΔN_{it} under NBRS is more complicated. As shown in Fig. 10(b), radiation induced electrons transport towards Si substrate under the applied negative electric field. Some of them fall into traps to form negative trapped oxide charges and cause a negative ΔN_{ot}. In the meantime, the applied negative electric field inhibit the motion of the radiation induced H^+ to the AlO_x/Si interface and hence the passivation (reaction (3)) at the interface will be suppressed. Nevertheless, the de-passivation (reaction (4)) can still occur and lead to an increase of ΔN_{it} if there is a source of hydrogen at the interface or in the Si substrate. For an n-type Si substrate, P-H complexes, or oxygen protrusions could be the possible source of hydrogen for de-passivation [49]. Furthermore, the energetic breaking of Si-H bonds through reaction (5) under BRS (process (3) in Fig. 10 (b)) could contribute to the increase of both ΔN_{ot} and ΔN_{it}. When a Si-H bond is broken, it will release H^+ which could be trapped in AlO_x to form an oxide trap under NBRS. Meanwhile, a Si dangling bond is formed and acts as an interface trap. The BRS could significantly reduce the binding energy of a H atom, indicating that the Si-H bond is relatively easy to break [29]. In addition, the defects or impurities, such as impurity Al atoms near the AlO_x/Si interface and suboxide bonds, could assist in the breaking of Si-H bonds and cause trapping of the H^+ released from the Si-H bonds under NBRS.

Consequently, under NBRS, the biased radiation induced electron trapping among AlO_x bulk results in a negative ΔN_{ot}. While the de-passivation, energetic break and assisted break of Si-H bonds by impurity Al atoms near the AlO_x/Si interface and suboxide bonds are the three main factors contribute a negative ΔN_{it}.

4. Conclusion

The effect of annealing temperature and biased γ-ray radiation stress on solution-processed AlO_x dielectrics has been systemically investigated in this paper. It has been found that a high annealing temperature of 300 ºC results in AlO_x thin films with low defect density, high metallic concentration, weak frequency dispersion, low interface trap density, low leakage current and good bias-stress stability. In addition, the stability of 300 °C-AlO_x based MOS capacitors under biased radiation stress was studied using an on-site technique with stress time up to 10^5 s and γ-ray exposure. The variation of oxide trap density in the AlO_x bulk and interface trap density at AlO_x/Si interface were calculated to better understand the trapping/de-trapping processes during biased radiation stress. The results suggest that ΔN_{ot} can be attributed to trapping/de-trapping behavior of radiation induced protons in AlO_x bulk, whilst ΔN_{it} is caused by the passivation/de-passivation of Si dangling bonds at AlO_x/Si interface. Furthermore, ΔN_{ot} and ΔN_{it} are of the order of 10^{-12} and 10^{-11} cm^{-2}, respectively, indicating that oxide trap charges are more effective than the interface trap charges in shifting V_{FB} for 300 °C-AlO_x MOS capacitor devices. It has been found that both ΔN_{ot} and ΔN_{it} increase under NBRS and decrease slightly under PBRS. When the device is under PBRS, the radiation induced electron and the passivation of Si dangling bonds at the AlO_x/Si interface, dominate the decrease of ΔN_{ot} and ΔN_{it}. On the other hand, the mechanism is more complicated. The de-passivation, energetic break and assisted break of Si-H bonds by impurity Al atoms near the AlO_x/Si interface and suboxide bonds are most likely to contribute to the increase in magnitude of ΔN_{ot} and ΔN_{it} under NBRS. In summary, the obtained results demonstrate that positive oxide trapped charge, Si dangling bonds and protons can have significant effects on the long-term reliability and biased ionizing radiation response in solution-processed AlO_x MOS capacitor devices.

Acknowledgement

This research was funded in part by the National Natural Science Foundation of China (21503169, 2175011441, and 61704111), Natural Science Foundation of Guangdong province (2017A030310524), Guangdong Research Center for Interfacial Engineering of Functional Materials (201701), Suzhou Science and Technology programme (SYG201623), Suzhou Industrial Park Initiative Platform Development for Suzhou Municipal Key Lab for New Energy Technology (RR0140), Natural Science Foundation of SZU (2017001), Key Program Special Fund in XJTLU (KSF-A-04, KSF-A-05, KSF-A-07, KSF-P-02 and KSF-T-03) and the XJTLU Research Development Fund (RDF-14-02-42 and RDF-17-01-13). The author IZM acknowledges UKRI GIAA award as well as British Council UKIERI project no. IND/CONT/G/17-18/18.

References

[1] W.Y. Xu, M.Z. Long, T.K. Zhang, L.Y. Liang, H.T. Cao, D.L. Zhu, J.B. Xu, Fully solution-processed metal oxide thin-film transistors via a low-temperature aqueous route, Ceram Int 43 (2017) 6130-6137.
[2] W.Y. Xu, H. Wang, L. Ye, J.B. Xu, The role of solution-processed high-κ gate dielectrics in electrical performance of oxide thin-film transistors, J Mater Chem C 2 (2014) 5389.
[3] H.S. Kim, P.D. Byrne, A. Facchetti, T.J. Marks, High performance solution-processed indium oxide thin-film transistors, J Am Chem Soc 130 (2008) 12580-12581.
[4] K. Song, W. Yang, Y. Jung, S. Jeong, J. Moon, A solution-processed yttrium oxide gate insulator for high-performance all-solution-processed fully transparent thin film transistors, J Mater Chem 22 (2012) 21265.
[5] E. Fortunato, P. Barquinha, R. Martins, Oxide semiconductor thin-film transistors: a review of recent advances, Adv Mater 24 (2012) 2945-2986.
[6] K. Nomura, H. Ohta, A. Takagi, T. Kamiya, M. Hirano, H. Hosono, Room-temperature fabrication of transparent flexible thin-film transistors using amorphous oxide semiconductors,

Nature 432 (2004) 488.
[7] J.S. Park, W.J. Maeng, H.S. Kim, J.S. Park, Review of recent developments in amorphous oxide semiconductor thin-film transistor devices, Thin Solid Films 520 (2012) 1679-1693.
[8] K.K. Banger, Y. Yamashita, K. Mori, R.L. Peterson, T. Leedham, J. Rickard, H. Sirringhaus, Low-temperature, high-performance solution-processed metal oxide thin-film transistors formed by a 'sol-gel on chip' process, Nat Mater 10 (2011) 45-50.
[9] C. Avis, Y.G. Kim, J. Jang, Solution processed hafnium oxide as a gate insulator for low-voltage oxide thin-film transistors, J Mater Chem 22 (2012) 17415.
[10] W.Y. Xu, H.T. Cao, L.Y. Liang, J.B. Xu, Aqueous Solution-Deposited Gallium Oxide Dielectric for Low-Temperature, Low-Operating-Voltage Indium Oxide Thin-Film Transistors: A Facile Route to Green Oxide Electronics, ACS Appl Mater Interfaces 7 (2015) 14720-14725.
[11] A. Liu, G.X. Liu, H.H. Zhu, B. Shin, E. Fortunato, R. Martins, F.K. Shan, Eco-friendly water-induced aluminum oxide dielectrics and their application in a hybrid metal oxide/polymer TFT, Rsc Adv 5 (2015) 86606-86613.
[12] G.H. Gelinck, H.E. Huitema, E. van Veenendaal, E. Cantatore, L. Schrijnemakers, J.B. van der Putten, T.C. Geuns, M. Beenhakkers, J.B. Giesbers, B.H. Huisman, E.J. Meijer, E.M. Benito, F.J. Touwslager, A.W. Marsman, B.J. van Rens, D.M. de Leeuw, Flexible active-matrix displays and shift registers based on solution-processed organic transistors, Nat Mater 3 (2004) 106-110.
[13] S. Wang, P.K. Ang, Z. Wang, A.L. Tang, J.T. Thong, K.P. Loh, High mobility, printable, and solution-processed graphene electronics, Nano Lett 10 (2010) 92-98.
[14] H. Wang, T.Y. Sun, W.Y. Xu, F.Y. Xie, L. Ye, Y.B. Xiao, Y. Wang, J. Chen, J.B. Xu, Low-temperature facile solution-processed gate dielectric for combustion derived oxide thin film transistors, RSC Adv. 4 (2014) 54729-54739.
[15] D.-H. Cho, S. Yang, C. Byun, J. Shin, M.K. Ryu, S.-H.K. Park, C.-S. Hwang, S.M. Chung, W.-S. Cheong, S.M. Yoon, H.-Y. Chu, Transparent Al–Zn–Sn–O thin film transistors prepared at low temperature, Appl Phys Lett 93 (2008) 142111.
[16] Y.H. Hwang, J.H. Jeon, K.J. Seo, B.S. Bae, Solution-Processed, High Performance Aluminum Indium Oxide Thin-Film Transistors Fabricated at Low Temperature, Electrochem Solid St 12 (2009) H336-H339.
[17] M. Esro, G. Vourlias, C. Somerton, W.I. Milne, G. Adamopoulos, High-Mobility ZnO Thin Film Transistors Based on Solution-processed Hafnium Oxide Gate Dielectrics, Adv Funct Mater 25 (2015) 134-141.
[18] P.D. Ye, G.D. Wilk, B. Yang, J. Kwo, S.N.G. Chu, S. Nakahara, H.J.L. Gossmann, J.P. Mannaerts, M. Hong, K.K. Ng, J. Bude, GaAs metal–oxide–semiconductor field-effect transistor with nanometer-thin dielectric grown by atomic layer deposition, Appl Phys Lett 83 (2003) 180-182.
[19] R. Branquinho, D. Salgueiro, L. Santos, P. Barquinha, L. Pereira, R. Martins, E. Fortunato, Aqueous combustion synthesis of aluminum oxide thin films and application as gate dielectric in GZTO solution-based TFTs, ACS Appl Mater Interfaces 6 (2014) 19592-19599.
[20] W.Y. Xu, H. Wang, F. Xie, J. Chen, H.T. Cao, J.B. Xu, Facile and environmentally friendly solution-processed aluminum oxide dielectric for low-temperature, high-performance oxide thin-film transistors, Acs Appl Mater Inter 7 (2015) 5803-5810.
[21] G.M. Huang, L. Duan, G.F. Dong, D.Q. Zhang, Y. Qiu, High-mobility solution-processed tin oxide thin-film transistors with high-kappa alumina dielectric working in enhancement mode, ACS Appl Mater Interfaces 6 (2014) 20786-20794.
[22] S.T. Meyers, J.T. Anderson, D. Hong, C.M. Hung, J.F. Wager, D.A. Keszler, Solution-processed aluminum oxide phosphate thin-film dielectrics, Chem Mater 19 (2007) 4023-4029.
[23] W. Yang, K. Song, Y. Jung, S. Jeong, J. Moon, Solution-deposited Zr-doped AlOx gate dielectrics enabling high-performance flexible transparent thin film transistors, J Mater Chem C 1 (2013) 4275.
[24] S.Y. Je, B.G. Son, H.G. Kim, M.Y. Park, L.M. Do, R. Choi, J.K. Jeong, Solution-processable LaZrOx/SiO_2 gate dielectric at low temperature of 180 degrees C for high-performance metal oxide field-effect transistors, ACS Appl Mater Interfaces 6 (2014) 18693-18703.
[25] C. Avis, J. Jang, High-performance solution processed oxide TFT with aluminum oxide gate dielectric fabricated by a sol–gel method, J Mater Chem 21 (2011) 10649.
[26] S. Guha, E. Cartier, N.A. Bojarczuk, J. Bruley, L. Gignac, J. Karasinski, High-quality aluminum oxide gate dielectrics by ultra-high-vacuum reactive atomic-beam deposition, J Appl Phys 90 (2001) 512-514.
[27] B. Park, D. Ho, G. Kwon, D. Kim, S.Y. Seo, C. Kim, M.-G. Kim, Solution-Processed Rad-Hard Amorphous Metal-Oxide Thin-Film Transistors, Adv Funct Mater 28 (2018) 1802717.

[28] R. Lok, S. Kaya, H. Karacali, E. Yilmaz, The Co-60 gamma-ray irradiation effects on the Al/HfSiO4/p-Si/Al MOS capacitors, Radiat Phys Chem 141 (2017) 155-159.
[29] X.J. Zhou, D.M. Fleetwood, L. Tsetseris, R.D. Schrimpf, S.T. Pantelides, Effects of Switched-bias Annealing on Charge Trapping in HfO_2 Gate Dielectrics, IEEE T Nucl Sci 53 (2006) 3636-3643.
[30] P. Barquinha, L. Pereira, G. Goncalves, R. Martins, D. Kuscer, M. Kosec, E. Fortunato, Performance and Stability of Low Temperature Transparent Thin-Film Transistors Using Amorphous Multicomponent Dielectrics, J Electrochem Soc 156 (2009) H824-H831.
[31] G.D. Wilk, R.M. Wallace, J.M. Anthony, High-κ gate dielectrics: Current status and materials properties considerations, J Appl Phys 89 (2001) 5243-5275.
[32] J.H. Park, Y.B. Yoo, K.H. Lee, W.S. Jang, J.Y. Oh, S.S. Chae, H.K. Baik, Low-temperature, high-performance solution-processed thin-film transistors with peroxo-zirconium oxide dielectric, ACS Appl Mater Interfaces 5 (2013) 410-417.
[33] J.H. Park, K. Kim, Y.B. Yoo, S.Y. Park, K.-H. Lim, K.H. Lee, H.K. Baik, Y.S. Kim, Water adsorption effects of nitrate ion coordinated Al_2O_3 dielectric for high performance metal-oxide thin-film transistor, J Mater Chem C 1 (2013) 7166.
[34] P.N. Plassmeyer, K. Archila, J.F. Wager, C.J. Page, Lanthanum aluminum oxide thin-film dielectrics from aqueous solution, ACS Appl Mater Interfaces 7 (2015) 1678-1684.
[35] L.Q. Zhu, J. Sun, G.D. Wu, H.L. Zhang, Q. Wan, Self-assembled dual in-plane gate thin-film transistors gated by nanogranular SiO_2 proton conductors for logic applications, Nanoscale 5 (2013) 1980-1985.
[36] J.M. Kwon, J. Jung, Y.S. Rim, D.L. Kim, H.J. Kim, Improvement in negative bias stress stability of solution-processed amorphous In-Ga-Zn-O thin-film transistors using hydrogen peroxide, Acs Appl Mater Inter 6 (2014) 3371-3377.
[37] Q.Q. Zhuo, H.X. Liu, Z.N. Yang, H.M. Cai, Y. Hao, The total dose irradiation effects of SOI NMOS devices under different bias conditions, Acta Physica Sinica 61 (2012) 6.
[38] J.A. Felix, D.M. Fleetwood, R.D. Schrimpf, J.G. Hong, G. Lucovsky, J.R. Schwank, M.R. Shaneyfelt, Total-dose radiation response of hafnium-silicate capacitors, IEEE T Nucl Sci 49 (2002) 3191-3196.
[39] A. Kahraman, E. Yilmaz, Irradiation response of radio-frequency sputtered Al/Gd_2O_3 /p-Si MOS capacitors, Radiat Phys Chem 139 (2017) 114-119.
[40] A. Kahraman, E. Yilmaz, A. Aktag, S. Kaya, Evaluation of Radiation Sensor Aspects o Er_2O_3 MOS Capacitors under Zero Gate Bias, IEEE T Nucl Sci 63 (2016) 1284-1293.
[41] M. Ceschia, A. Paccagnella, A. Cester, A. Scarpa, G. Ghidini, Radiation induced leakage current and stress induced leakage current in ultra-thin gate oxides, IEEE T Nucl Sci 45 (1998) 2375-2382.
[42] D.A. Neamen, Modeling of MOS Radiation and Post Irradiation Effects, IEEE T Nucl Sci 31 (1984) 1439-1443.
[43] T. Stanley, D. Neamen, P. Dressendorfer, J. Schwank, P. Winokur, M. Ackermann, K. Jungling, C. Hawkins, W. Grannemann, The Effect of Operating Frequency in the Radiation Induced Buildup of Trapped Holes and Interface States in MOS Devices, IEEE T Nucl Sci 32 (1985) 3982-3987.
[44] F. McLean, A framework for understanding radiation-induced interface states in SiO2 MOS structures, IEEE T Nucl Sci 27 (1980) 1651-1657.
[45] T.R. Oldham, F.B. McLean, Total ionizing dose effects in MOS oxides and devices, IEEE T Nucl Sci 50 (2003) 483-499.
[46] L. Tsetseris, X.J. Zhou, D.M. Fleetwood, R.D. Schrimpf, S.T. Pantelides, Physical mechanisms of negative-bias temperature instability, Appl Phys Lett 86 (2005) 142103.
[47] S.N. Rashkeev, D.M. Fleetwood, R.D. Schrimpf, S.T. Pantelides, Proton-induced defect generation at the Si-SiO_2 interface, IEEE T Nucl Sci 48 (2001) 2086-2092.
[48] S.N. Rashkeev, D.M. Fleetwood, R.D. Schrimpf, S.T. Pantelides, Defect Generation by Hydrogen at the Si/SiO_2 Interface, Phys Rev Lett 87 (2001) 165506.
[49] X.J. Zhou, L. Tsetseris, S.N. Rashkeev, D.M. Fleetwood, R.D. Schrimpf, S.T. Pantelides, J.A. Felix, E.P. Gusev, C. D'Emic, Negative bias-temperature instabilities in metal–oxide–silicon devices with SiO2 and SiOxNy/HfO2 gate dielectrics, Appl Phys Lett 84 (2004) 4394-4396.